AN EDGE-PRESERVING ACTIVE CONTOUR MODEL WITH BILATERAL FILTER BASED ON HYPERSPECTRAL IMAGE SPECTRAL INFORMATION FOR OIL SPILL SEGMENTATION

Wandi Wang[1], Hui Sheng[1], Shanwei Liu[1], Yanlong Chen[1], Jianhua Wan[1], Jijun Mao[2]*

1. China University of Petroleum, Qingdao 266580, China.
2. Surveying and Mapping Institute of Shandong Province, Jinan 250102, China

ABSTRACT

The oil spill creating potentially serious environmental impacts on both marine life and the coastal shorelines. Accurately oil spill monitoring can reduce economic loss and assess these impacts. With the development of imaging technology, high spectral resolution data in hyperspectral imagery (HSI) sensors provide a valuable source of information that can be used for oil spill area segmentation by semi-automatic methods. At present, there are many methods for oil spill segmentation, most of which are based on threshold or neural network. These methods can achieve better segmentation results when the oil spill image is clear, but do not effectively segment the oil spill area when the image with high noisy and the oil spill area is blurred. In this article, for hyperspectral images blurred with high noisy, a BF-MD-LBF model is proposed. There are two key steps in the proposed method: (1) To take advantage of spectral information, KPCA is introduced to Local Binary Fitting (LBF) energy function and a new energy function model is constructed; (2) To have hyperspectral image smoothed without blurring the edges, the bilateral filter is incorporated into the LBF energy function as regularization term.

Index Terms—LBF, hyperspectral image, bilateral filter, KPCA

1. INTRODUCTION

Marine oil spill accidents, which have caused various types of environmental damage, have frequently occurred at different scales [1-2]. Countries around the world have strengthened their monitoring of and research on marine oil spills due to the potential endangerment of marine ecosystems, environment fisheries, and wildlife, as well as other societal interests. Previous studies indicate that hyperspectral remote sensing technology is an effective method to monitor oil spills on water. [3-7]. Active contour model (ACM) is a robust segmentation method that has been widely used in object extraction from remote sensing images, recently. Ball proposed a supervised hyperspectral classification procedure using best band [8]. Zhou proposed a modified C-V level set method classified hyperspectral image [9]. Li proposed two fast LSEs for man-made object extraction from high spatial resolution remote sensing images [10]. Liasis developed and applied a new active contour model for building extraction [11]. Sun combined CNN and ACM solutions at extracting building boundaries from high-resolution optical images [12].

According to previous studies, the active contour model is suitable for processing hyperspectral images, but only for single spectral band image. In addition, active contour model based on the local or global gray information of the image. The difference of grayscale information in each spectral segment results in different segmentation results, which lead to the loss of spectral information and the reduction of segmentation accuracy. In this study, a new BF-MD-LBF model is proposed to solve the above issues. The rest of this paper is organized as follows. Section 2 describes our methods. Section 3 compares our method with other methods on data.

2. METHOD

2.1 Local Binary Fitting (LBF) model

Let ϕ be a contour in the image domain Ω. For each point $x \in \Omega$, The LBF energy functional is defined by [13]

$$\begin{aligned} &E_x^{LBF}(\phi, f_1(x), f_2(x)) = \\ &\lambda_1 \int_{in(\phi)} K(x-y) \,|\, I(y) - f_1(x) \,|^2\, M_1(\phi(y))dy \\ &+\lambda_2 \int_{out(\phi)} K(x-y) \,|\, I(y) - f_2(x) \,|^2\, M_2(\phi(y))dy \end{aligned} \quad (1)$$

where λ_1 and λ_2 are positive balancing constants, separately, $I(y)$ is the original image, $f_1(x)$ and $f_2(x)$ are characterizes the weighted averages of the intensities in a neighborhood of (x, y). $M_1(\phi) = H(\phi)$, $M_2(\phi) = 1 - H(\phi)$, and $H(\phi)$ is the Heaviside function. $K(x-y)$ is the gaussian kernel:

$$K_\sigma(x) = \frac{1}{(2\pi)^{n/2}\sigma^n} e^{-|x|^2/2\sigma^2} \quad (2)$$

For the image domain Ω. The RSF energy functional is defined by

$$E(\phi, f_1, f_2) = \int_\Omega E_x^{LBF}(\phi, f_1(x), f_2(x))dx \quad (3)$$

Keeping f_1 and f_2 fixed, and minimizing the energy functional $E(\phi, f_1, f_2)$ with respect to ϕ, we derive the gradient descent flow:

$$\int K_\sigma(x-y) M_i(\phi(x))(I(y) - f_i(x))dy = 0 \quad (4)$$

$$f_i(x) = \frac{K_\sigma(x) * [H_\varepsilon(\phi(x))I(x)]}{K_\sigma(x) * H_\varepsilon(\phi(x))}, i = 1, 2 \quad (5)$$

2.2 Multi-band active contour model based on LBF model

Let Ω_j be the hyperspectral image, j is the number of the bands selected, x_j is pixel vector, Figure 1 shows the pixel vector x_j in detail.

Since the reflectance of the various kinds of oil spills peak in the spectral range from 500 to 580 nm (Zhang et al. 2000, Zhao and Cong 2000), 35 bands from 178-213 of experimental hyperspectral data were selected to process images in this study [13-14].

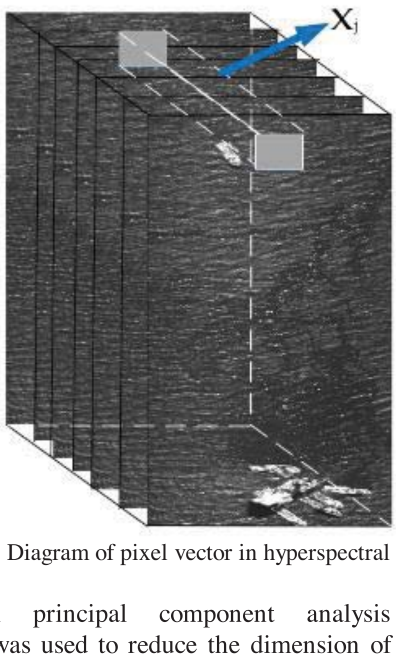

Figure 1. Diagram of pixel vector in hyperspectral imagery

Kernel principal component analysis (KPCA) algorithm was used to reduce the dimension of the vector and return the principal component value $P(x, y)$. $P(x, y)$ can be defined as:

$$P(x, y) = f_i^T v_i, i = 1, 2 \quad (6)$$

where f_i is the vector matrix, and v is the feature vector of matrix.

Now, $f_1(x)$ and $f_2(x)$ are redefined as:

$$f_i^P(x, y) = \begin{cases} i_i(x, y) = \dfrac{K_\sigma(x) * [H_i(\phi(x))I(x)]}{K_\sigma(x) * H_i(\phi(x))} \\ P_i(x, y) = \dfrac{K_\sigma(x) * [H_i(\phi(x))P(x)]}{K_\sigma(x) * H_i(\phi(x))} \end{cases}, i = 1, 2 \quad (7)$$

where K_σ is the gaussian function with a standard deviation of σ, and * represents the convolution operator.

Then, energy functional is redefined as:

$$\begin{aligned} &E_x^P(\phi, f_1^P(x), f_2^P(x)) = \\ &\lambda_1 \int_{in(\phi)} K(x-y) | I(y) - f_1^P(x) |^2 M_1(\phi(y))dy \\ &+\lambda_2 \int_{out(\phi)} K(x-y) | I(y) - f_2^P(x) |^2 M_2(\phi(y))dy \end{aligned} \quad (8)$$

In order to ensure stable evolution of the level set function ϕ, the distance regularizing term was added. Distance regularizing term is defined by

$$P(\phi) = \int_\Omega \frac{1}{2}(|\nabla\phi(x) - 1|)^2 dx \sqrt{a^2 + b^2} \quad (9)$$

To regularize the zero level contour of ϕ, it also need the length of the zero level curve (surface) of ϕ, which is given by

$$L(\phi) = \int_\Omega \delta(\phi(x)) |\nabla\phi(x)| dx \quad (10)$$

The entire MDLBF energy functional is defined by

$$\begin{aligned} F(\phi, f_1(x, y), f_2(x, y)) = E_x^P(\phi, f_1^P(x), f_2^P(x)) \\ + \alpha P(\phi) + \beta L(\phi) \end{aligned} \quad (11)$$

where α and β are nonnegative constants.

2.3 Bilateral filter regularization term

In this study, to have our hyperspectral image smoothed by the bilateral filter. Let I_d denote input image smoothed by bilateral filter. Let $\xi(x, y)$ denote a local square window around (x, y) in I_d and $|\xi(x, y)|$ is the number of pixels in $\xi(x, y)$. The local mean $\mu(x, y)$ and local variance $\sigma^2(x, y)$ of I_d within $\xi(x, y)$ are defined by

$$\mu(x, y) = \frac{1}{|\xi(x, y)|} \sum_{(u,v)\in\omega(x,y)} I_d(u, v) \quad (12)$$

$$\sigma^2(x, y) = \frac{1}{|\xi(x, y)|} \sum_{(u,v)\in\omega(x,y)} [I_d(u, v) - \mu(x, y)]^2 \quad (13)$$

The intermediate coefficients p(x, y) and q(x, y) are computed, respectively, as follows:

$$p(x,y)=\frac{\frac{1}{|\xi(x,y)|}\sum_{(u,v)\in\omega(x,y)}|I_d(u,v)|^2-|\mu(x,y)|^2}{\sigma^2(x,y)+\in} \tag{14}$$

$$q(x,y)=\mu(x,y)(1-p(x,y)) \tag{15}$$

where $\in$ is a regularization parameter preventing $p(x,y)$ from being too large. The mean maps $\overline{p}$ and $\overline{q}$ for p and q are computed as follows:

$$\overline{p}(x,y)=\frac{1}{|\xi(x,y)|}\sum_{(u,v)\in\omega(x,y)}p(u,v) \tag{16}$$

$$\overline{q}(x,y)=\frac{1}{|\xi(x,y)|}\sum_{(u,v)\in\omega(x,y)}q(u,v) \tag{17}$$

Finally, one filtered image pixel $\hat{I}_d(x,y)$ is given by

$$\hat{I}_d(x,y)=\overline{p}(x,y)I_d(x,y)+\overline{q}(x,y) \tag{18}$$

The bilateral filter was incorporated into the LBF energy functional by introducing the following regularization term:

$$\begin{aligned}R_B(\phi)=&\gamma_1\iint\left|\nabla\hat{I}_d(x,y)\right|H_\in(\phi(x,y))dxdy\\&+\gamma_2\iint\left|\nabla H_\in(\phi(x,y))\right|\hat{I}_d(x,y)dxdy\end{aligned} \tag{19}$$

where γ_1 and γ_2 are positive constants, which balance the two terms for bilateral filter preserving regularization in formula (19).

2.4 BF-MD-LBF model energy functional

The bilateral filter regularization term is integrated into the BD-LBF for segmenting oil spills in hyperspectral images, which is given as BF-BD-LBF by

$$\begin{aligned}F(\phi,f_1(x),f_2(x))=&E^{MD}(\phi,f_1(x),f_2(x))\\&+\alpha P(\phi)+\beta L(\phi)+\tau R_B(\phi)\end{aligned} \tag{20}$$

where α , β and, τ are nonnegative constants.

3. EXPERIMENT

In order to validate the performance of the proposed model, experiments were executed on two hyperspectral data sets. First scene was gathered by AVIRIS sensor over the Indian Pines test site in North-western Indiana and consist 224 spectral reflectance bands. Second scene was obtained on June 11th, 2011 at Bohai Sea Penglai 19–3 Oil field and consist 258 spectral reflectance bands.

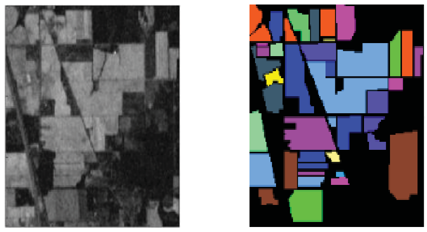

Indian pines dataset　　Ground truth

Figure 2. Indian pines dataset and ground truth

(a)　(b)　(c)

Figure 3. Segmentation results by BF-BD-LBF

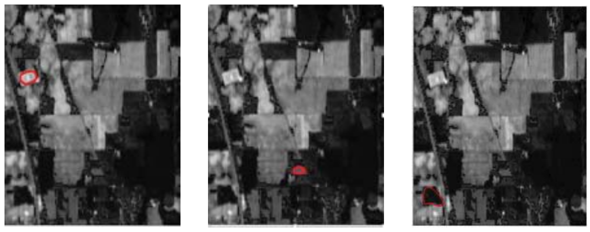

(a)　(b)　(c)

Figure 4. Segmentation results by LBF

Table 1. Accuracy assessment

	BF-BD-LBF			LBF		
Ground object type	16	7	14	16	7	14
OA (%)	96	91	91	85	83	80
Kappa	0.90	0.86	0.93	0.73	0.69	0.64

The 7th, 14th and 17th ground objects were segmented by the model proposed in this paper. The segmentation results by BF-BD-LBF and LBF are shown in Figure 3 and Figure 4, respectively. Table 1 records the *OA* and *kappa* coefficients of the experimental results, where the larger the *OA* and *kappa* values, the higher the accuracy of the segmentation results. It can be seen from Table 3 that the segmentation performance of the BF-BD-LBF model is better than LBF model.

To validate the performance of the proposed model for oil spill segmentation, experiment were executed on second scene, compared with LBF [15], CV [16] , DRLSE [17],K-means [18], Region growing [19], KI [20], OTSU [21], and Watershed [22] method.

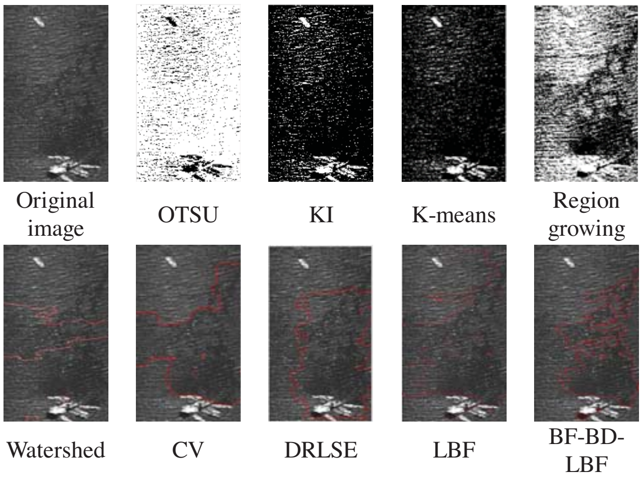

Figure 5. Original image and oil spills segmentation results of 10 different methods.

It can be clearly seen from figure 5 that the hyperspectral oil spill image contains a large number of bright spots and shadow noises. The segmentation results of the KI, OTSU, and K-means methods are poor in continuity and integrity. The segmentation effect of the region growing method is improved compared with the above three algorithms, but the integrity of the segmentation result is still not good. These four kinds of methods are all pixel-based image segmentation methods, so the segmentation process is susceptible to the effects of bright spots and shadow noise in the image. DRLSE algorithm could not distinguish between oil spills and ships. The segmentation result of the watershed algorithm is also not good. LBF and CV model could more accurately find the boundary on the left side of the oil spill area, but could not find the boundary on the right side of the oil spill area, and there are many wrong contours. The BF-MD-LBF model, which proposed in this paper, could segment the oil spill area more accurately, and there are only a few mis-segmented areas.

4. CONCLUSION

This paper proposed an active contour model based on LBF model, which consider the HSI spatial and spectral information of hyperspectral image and could effectively reduce noise. Experiments indicate that the proposed method could get a well segmentation result of oil spills using the blurred hyperspectral image, which could greatly decrease noise and make full use of spectral information.

5. ACKNOWLEDGMENTS

This research has been supported by the National Key R&D program (2017YFC1405600), National natural science foundation of China (41776182), and Natural Science Foundation of Shandong Province (ZR2016DM16, ZR2019MD023).

6. REFERENCES

[1] Rischard J F, "High Noon: We Need New Approaches to Global Problem-Solving, Fast," *Journal of International Economic Law*, vol. 44, no. 3, pp. 507-525, 2001.

[2] Chiau W Y, "Changes in the marine pollution management system in response to the Amorgos oil spill in Taiwan," *Marine pollution bulletin*, vol. 51, pp. 1041-1047, 2005.

[3] Khanna S, Santos M, and Ustin S, "Comparing the potential of multispectral and hyperspectral data for monitoring oil spill impact," Sensors, vol. 18, no. 2, pp. 558, 2018.

[4] Fingas M, and Brown C, "A review of oil spill remote sensing," *Sensors*, vol. 18, no. 1, pp. 91, 2018.

[5] Ahmadi, Salman, "Automatic urban building boundary extraction from high resolution aerial images using an innovative model of active contours," *International Journal of Applied Earth Observation and Geoinformation,* vol. 12, no. 3, pp. 150-157, 2010.

[6] Salem F, Kafatos M, and El-Ghazawi T, "Hyperspectral image analysis for oil spill detection," *Summaries of NASA. JPL Airborne Earth Science Worksho*p, pp. 5-9, 2001.

[7] Lu Y, Tian Q, and Wang X, "Determining oil slick thickness using hyperspectral remote sensing in the Bohai Sea of China," *International Journal of Digital Earth*, vol. 6, no. 1, pp. 76-93, 2013.

[8] Ball J E, and Bruce L M, "Level set hyperspectral image classification using best band analysis," *IEEE Transactions on Geoscience and Remote Sensing*, vol. 45, no. 10, pp. 3022-3027, 2007.

[9] Zhou S, Zhang X, and Zhang J, "Spectral-spatial classification of hyperspectral image based on semi-supervised and level set methods,"*2012 IEEE International Geoscience and Remote Sensing Symposium,* pp. 4279-4282, 2012.

[10] Li, Zhongbin, "Extracting man-made objects from high spatial resolution remote sensing images via fast level set evolutions," *IEEE Transactions on Geoscience and Remote Sensing*, vol. 53, no. 2, pp. 883-899, 2015.

[11] Liasis, Gregoris, and Stavros Stavrou, "Building extraction in satellite images using active contours and colour features,"

International Journal of Remote Sensing, vol. 37, no. 5, pp. 1127-1153, 2016.

[12] Sun, and Ying, "Extracting building boundaries from high resolution optical images and LiDAR data by integrating the convolutional neural network and the active contour model," *Remote Sensing,* vol. 10, no. 9, pp. 1459, 2018.

[13] Zhang Y, "Analysis of oil film spectrum and monitoring oil spilled by remote sensing," *Marine environmental science. Haiyang Huanjing Kexue*, Dalian, vol. 19, no. 3, pp. 5-10, 2000.

[14] Dongzhi Z, and Peifu C, "The research of visual light wave-band feature spectrum of sea-surface oil spill," *Remote Sensing Technology and Application (in Chinese)*, vol. 15, no. 3, pp. 160-164, 2000.

[15] Li C, Kao C Y, and Gore J C, "Implicit active contours driven by local binary fitting energy," *2007 IEEE Conference on Computer Vision and Pattern Recognition,* pp. 1-7, 2007.

[16] Chan T F, and Vese L A, "Active contours without edges," *IEEE Transactions on image processing*, vol. 10, no. 2, pp. 266-277, 2001.

[17] Li C, Xu C, and Gui C, "Distance regularized level set evolution and its application to image segmentation," *IEEE transactions on image processing*, vol. 19, no. 12, pp. 3243-3254, 2010.

[18] MacQueen J, "Some methods for classification and analysis of multivariate observations," *Proceedings of the fifth Berkeley symposium on mathematical statistics and probability*, vol. 1, no. 14, pp. 281-297, 1967.

[19] Pal N R, and Pal S K, "A review on image segmentation techniques," *Pattern recognition*, vol. 29, no. 9, pp. 1277-1294, 1993.

[20] Kittler J, and Illingworth J, "Minimum error thresholding," *Pattern recognition*, vol. 19, no. 1, pp. 41-47, 1986.

[21] Pratt W K, and Adams J E, "Digital Image Processing, 4th Edition," *Journal of Electronic Imaging*, vol. 16, no. 2, pp. 131-145, 2007.

[22] Beucher S, "Use of watersheds in contour detection," *Proceedings of the International Workshop on Image Processing.* 1979.